Gold nanoparticles dispersed into poly(aminothiophenol) as a novel electrocatalyst—Fabrication of modified electrode and evaluation of electrocatalytic activities for dioxygen reduction

Anantha Iyengar Gopalan [a,b,c], Kwang-Pill Lee [a,b,*], Kalayil Manian Manesh [a], Padmanaban Santhosh [a], Jun Heon Kim [a,b]

[a] *Advanced Analytical Science and Nanomaterials Laboratory, Department of Chemistry Education, Kyungpook National University, Daegu 702-701, South Korea*
[b] *Nano Practical Application Center, Daegu 704-230, South Korea*
[c] *Department of Industrial Chemistry, Alagappa University, Karaikudi-630003, India*

Abstract

Gold nanoparticles were embedded into an electroactive polymer layer to modify the glassy carbon (GC) electrode and to fabricate a novel catalyst electrode. Cyclic voltammetry was performed to form the electroactive polymer, poly(aminothiophenol), PATP and deposit the Au^0 nanoparticles, simultaneously. 4-Aminothiophenol (ATP) was converted into an inclusion complex with β-cyclodextrin and used to form the electroactive layer on the surface of GC electrode. Au^0 nanoparticles were incorporated into film of PATP simultaneously by the electrolysis of a solution of $HAuCl_4$. Thus, newer catalyst electrode, PATP-Au_{nano}, was fabricated. The scanning probe microscopic image of PATP-Au_{nano} indicates the presence of uniformly distributed Au^0 nanoparticles of the sizes ∼10 nm. Electroactivity of PATP-Au_{nano} for reduction of dioxygen (O_2) was evaluated in O_2 saturated solution. Cyclic voltammetry was used to demonstrate the enhanced electrocatalytic activity of the PATP-Au_{nano}. A reduction peak at ∼430 mV with an enhanced peak current was observed for the oxygen reduction reaction (ORR) in O_2 saturated 0.5 M sulfuric acid solution. A more positive onset potential and higher catalytic current for ORR are the striking features of PATP-Au_{nano} catalyst. Double potential chronoamperometry, rotating disc (RDE) and rotating ring–disk electrode (RRDE) experiments were carried out to investigate the kinetic parameters of ORR on this electrode. Results from RDE and RRDE voltammetry experiments demonstrate that ORR on the PATP-Au_{nano} is a four electron and diffusion controlled process with a catalytic rate constant of $3.65 \times 10^3 \, M^{-1} \, s^{-1}$ and a diffusion coefficient of $7.82 \times 10^{-5} \, cm^2 \, s^{-1}$.
© 2006 Elsevier B.V. All rights reserved.

Keywords: Gold nanoparticles; Electroactive film; Glassy carbon electrode; Oxygen reduction

1. Introduction

Materials generated from the incorporation of metal (Au/Pt/Pd) nanoparticles into polymer matrix receive substantial research interest directed to the development of hybrid materials of new catalytic [1–3], electronic and optoelectronic [4,5] functionalities. Specifically, loading of metallic particles into the matrix of a conducting polymer such as polyaniline [4,6] receives interest due to the electronic interactions between nanoparticles and groups in the conducting polymer. As a result of molecular interactions, the electrocatalytic properties of nanoparticles are significantly improved [7].

Gold nanoparticles anchored into certain substrates show catalytic activity for many reactions [8,9]. In particular, Au nanoparticles protected via self-assembly in two- or three-dimensional lattices are showing promise for the construction of nanodevices and nanocircuits [10,11]. Since the report by Brust et al. [12], Au nanoclusters covered by self-assembled monolayers of alkanethiols have attracted the attention of many research groups. Au nanoparticles were also found to have enhanced electrocatalytic activities toward the electrochemical reduction of dioxygen (O_2) in acidic media [13,14], catalytic hydrogenation of unsaturated alcohols and aldehydes [15] and low-temperature

* Corresponding author. Tel.: +82 539505901; fax: +82 539528104.
E-mail addresses: algopal_99@yahoo.com (A.I. Gopalan), kplee@knu.ac.kr (K.-P. Lee).

oxidation of carbon monoxide [16]. While hydrophilic substrates are ideally suited to anchor Au particles, carbon based substrates require sufficient modifications prior to loading of Au nanoparticles. However, the process is tedious and involves multiple steps.
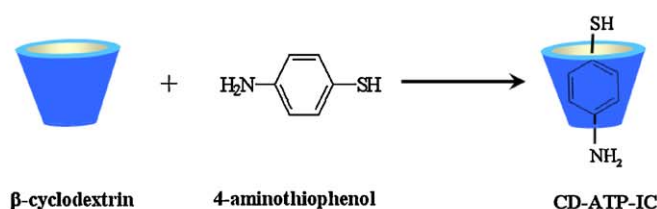
Glassy carbon (GC) electrodes are characterized by their high chemical inertness as well as low oxidation rate in addition to low gas and liquid permeability [17]. These properties render GC electrode a suitable base for the loading of various metal particles or polymer thin films. Such modified catalyst electrodes are expected to have improved electrocatalytic activity toward several electrochemical applications [18,19] in comparison to the bulk electrode. However, it is difficult to deposit

metal nanoparticles directly onto the GC electrode due to its hydrophobic nature. Hence, an additional procedure is required to immobilize nanocatalysts into these type of substrates to form one-dimensional (1D) or two-dimensional (2D) nanostructures [20]. Au nanoparticles deposited onto the solid supports exhibit useful catalytic and electrocatalytic properties. Moreover, the catalytic activity of Au nanoparticles significantly depends on the sizes [21]. Recently, many studies related to size control of Au nanoparticles, their composition, and their self-assembly or self-organization into 2D and 3D structures have been reported [22,23].

Conducting polymers are known to have wide variety of applications like sensors [24], cathode material of a lithium
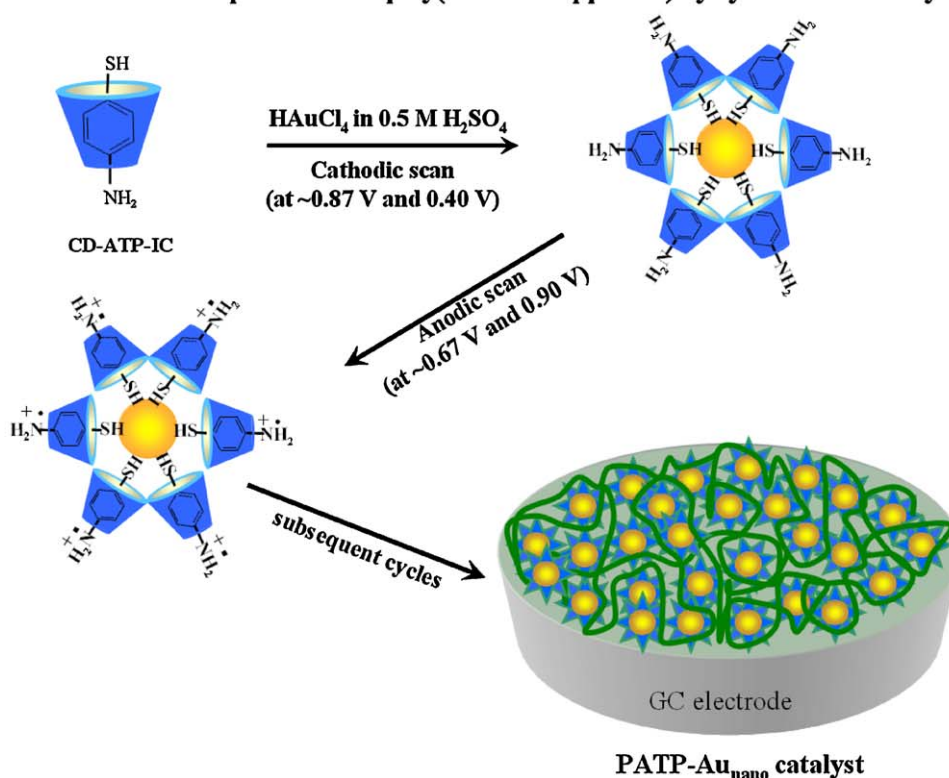
Fabrication of PATP-Au_nano catalyst through a cyclic electrochemical process

(a) **Formation of inclusion complex of β-cyclodextrin with 4-aminothiophenol**

(b) **Electrochemical steps for the sequential formation of**
Au⁰ nanoparticles and poly(4-aminothipphenol) by cyclic voltammetry

Scheme 1. Fabrication of PATP-Au_nano catalyst through a cyclic electrochemical process. (a) Formation of inclusion complex of β-cyclodextrin with 4-aminothiophenol and (b) electrochemical steps for the sequential formation of Au⁰ nanoparticles and poly(4-aminothiophenol) by cyclic voltammetry.

secondary battery [25], electrocatalysts [26], microelectronic devices [27], etc., due to their interesting electrochemical properties. The porous structure of the conducting polymer allows to disperse the catalyst particles into the polymer matrix and generate new catalytic and electrocatalytic sites [28,29]. Conducting polymers with dispersed metal nanoparticles have shown properties of the individual components with a synergistic effect.

Various approaches have been developed for the fabrication of electrocatalysts in the form of films [30]. Layer-by-layer methods are adopted extensively, which involve covalent bonding [31], electrostatics [32,33] and ligand–metal ion–ligand bridges [34]. However, these procedures of fabricating modified catalyst electrodes require several steps. The method of fabrication of modified electrocatalysts in a single step through simultaneous deposition of the supporting layer and metal nanoparticles on the solid surface is not yet reported.

In the present investigation, a novel electrocatalyst was prepared by uniformly dispersing Au^0 nanoparticles into in situ generated poly(aminothiophenol), PATP film via thiol interactions. Cyclic voltammetry was used to deposit simultaneously the film of PATP and Au^0 nanoparticles in a sequential process (Scheme 1). Surface of GC was modified with this electrocatalyst to fabricate a modified electrode, PATP-Au$_{nano}$ and the electrocatalytic activity of the modified electrode toward ORR was investigated. The PATP-Au$_{nano}$ possesses excellent electroactivity for ORR. Other electrochemical techniques such as double potential chronoamperometry and rotating ring–disk electrode were employed to investigate the kinetic parameters of ORR on the PATP-Au$_{nano}$ catalyst.

2. Experimental

2.1. Materials

β-Cyclodextrin (CD), 4-aminothiophenol (ATP), auric acid and sulfuric acid of analytical grades were used as received. Double-distilled water was used throughout the experiments.

2.2. Formation of inclusion complex

The inclusion complex of CD with ATP was prepared by adopting the procedure detailed in the literature [35]. In a typical synthesis of the inclusion complex, about 0.0626 g of ATP was dissolved in 10 mL of ethanol and added to an aqueous solution containing 0.5676 g of CD in 40 mL of water. A homogenous solution was obtained after stirring. After distilling off the solvents under reduced pressure, a white powder, inclusion complex of β-cyclodextrin with 4-aminothiophenol (CD-ATP-IC) (Scheme 1a) was collected. The powder was washed with acetone to remove the excess of ATP and dried to produce the powder of CD-ATP-IC. The formation of inclusion complex was ascertained by FT-IR and ^{1}H NMR spectroscopic measurements.

2.3. Fabrication of PATP-Au$_{nano}$ catalyst

A suspension was prepared by dissolving 50 mg of the inclusion complex (CD-ATP-IC) in 10 mL DMF. Five microliter of the suspension was dropped on the surface of the glassy carbon (GC) electrode and kept at 60 °C for 12 h to evaporate the solvent. The electrode was washed with water and stored under nitrogen atmosphere. Gold particles were electrochemically deposited into the GC/CD-ATP-IC electrode surface from 0.5 M H$_2$SO$_4$ solution containing 2.0×10^{-4} M HAuCl$_4$ by applying a repetitive potential scan between 1.0 and −0.1 V (versus SCE) at a scan rate of 50 mV s^{-1} for 'n' cycles, (n was varied to deposit different amount of Au^0 particles). Poly(aminothiophenol) (PATP) and Au^0 particles were simultaneously formed on the GC electrode. Thus, the modified electrode (PATP-Au$_{nano}$) was fabricated. Formation of PATP-Au$_{nano}$ is illustrated in Scheme 1b. PATP-Au$_{nano}$ with different Au^0 loading were also fabricated.

2.4. Characterization

The surface topography of the PATP-Au$_{nano}$ was examined using scanning probe microscopy, SPM (Digital Instruments; Nanoscope Multimode) in the tapping mode with standard silicon nitride tips. X-ray photoelectron spectroscopy, XPS was recorded on VG Microtech and MT 500/L with a Mo Kα X-ray radiation as the X-ray source for excitation. The data were obtained at room temperature and the operating pressure in the analysis chamber was below 10^{-9} Torr with an analyzer pass energy of 50 eV. The resolution was 0.2 eV.

2.5. Electrochemical measurements

The electrochemical experiments were carried out using a EG&G PAR electrochemical analyzer. The electrochemical experiments were performed in a standard single-compartment electrochemical cell that contained the PATP-Au$_{nano}$ as working electrode, SCE and platinum wire were used as reference and auxiliary electrodes, respectively.

Cyclic voltammograms (CVs) were recorded between +1.0 and 0 V versus SCE at a scan rate of 50 mV s^{-1} in O$_2$ or Ar saturated 0.5 M H$_2$SO$_4$ solution. Double potential chronoamperograms were obtained by setting the first and second working electrode potential at 800 and 0 mV (versus SCE), respectively. In the case of rotating ring–disc electrode (RRDE) measurements, a platinum ring and PATP-Au$_{nano}$ modified GC as disc electrode were used.

3. Results and discussion

3.1. Fabrication of PATP-Au$_{nano}$ catalyst electrode

Electrocatalytic Au^0 nanoparticles loaded GC modified electrode assembly, PATP-Au$_{nano}$ catalyst (designated as PATP-Au$_{nano}$), was fabricated by the methodology represented in Scheme 1. Generally, it is difficult to deposit Au^0 particles onto a bare GC electrode. A supporting matrix is required to anchor Au^0 particles on the surface of GC. Toward this, an electroactive polymer film can be deposited onto the surface of GC and subsequently Au^0 particles can be deposited over the film of electroactive polymer in a separate step. Otherwise, to fabricate a Au^0 modified catalytic GC electrode, two independent elec-

trochemical processes are needed. The modified electrode thus formed would have two layers; a supporting layer for anchoring Au^0 particles and a layer of Au^0 particles. Unless a strong electrostatic binding exists between Au^0 particles and the supporting layer, the bilayer modified Au^0 electrocatalyst may not be compatible under electrochemical operations. Hence, it is essential to have a supporting matrix on GC that would disperse and anchor Au^0 particles.

In the present study, we have used an electrochemical technique, cyclic voltammetry, for the simultaneous formation of film of an electroactive polymer and deposition of Au^0 nanoparticles onto the surface of GC. The electroactive film PATP was formed by the oxidation of ATP present in the layer of CD-ATP-IC on the surface of GC and Au^0 particles were deposited by the reduction of $HAuCl_4$ from the electrolyte solution (Scheme 1). Further, Au^0 particles in the electroactive films are stabilized through interactions with –SH groups (Scheme 1). Importantly, the electroactive polymer film, PATP was in situ formed as a film on the surface of GC electrode and Au^0 nanoparticles are stabilized and anchored into the film to obtain the novel electrocatalyst, PATP-Au_{nano}. The electrochemistry involved in the formation of PATP-Au_{nano} is described below.

CD-ATP-IC coated GC electrode was kept in a solution containing 2.0×10^{-4} M $HAuCl_4$ (in 0.5 M H_2SO_4) and cyclic voltammograms were recorded by scanning the potential from -100 to 1000 mV at a scan rate of 50 mV s^{-1} (Fig. 1). Interestingly, during the anodic potential scan, two peaks were observed, at 0.67 and 0.90 V, with the increase in peak current with number of potential cycles. The two peaks signify the formation of a layer of PATP on the surface of the GC electrode. During the cathodic potential, two peaks were observed at ∼0.87 and ∼0.40 V. The initial broad peak at 0.87 V is attributed to the reduction of adsorbed $AuCl_4^-$ ions to Au^0 [36]. These observations clearly suggest the successive formation of film of conducting polymer and incorporation of Au^0 particles. As a result, the PATP-Au_{nano} catalyst was fabricated.

It must be noted that electropolymerization of a solution of ATP did not give any electroactive film. Hence, we propose the mechanism of modification of GC electrode with simultaneous formation of electroactive polymer film, PATP and Au^0 particles as follows. ATP may have adequate configuration to convert
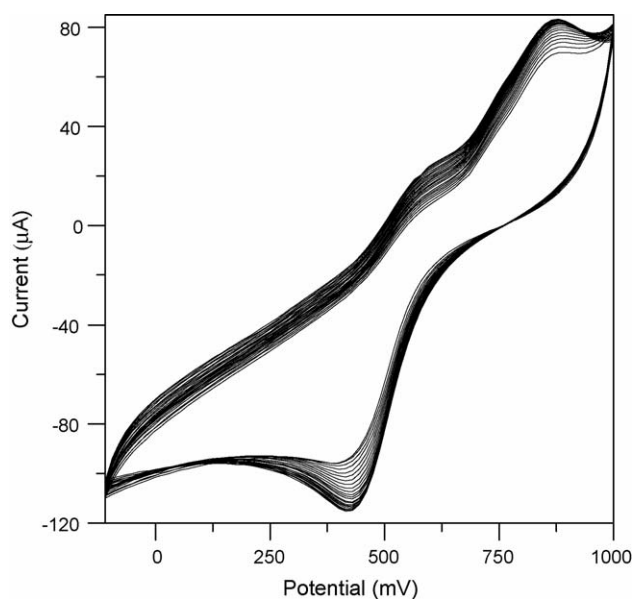

Fig. 1. Cyclic voltammograms of CD-ATP-IC coated GC electrode in the 0.5 M H_2SO_4 solution containing 2.0×10^{-4} M $HAuCl_4$ (inset shows the first cycle); scan rate: 50 mV s^{-1}.

into PATP when it is present as a self-assembled layer on the flat surface or Au^0 atoms [37]. Hence, in the present study, the self-assembly of ATP was hastened by anchoring the inclusion complex, CD-ATP-IC over Au atoms (Scheme 1).

The peaks observed at 0.67 and 0.90 V in CVs (Fig. 1) corresponding to the fabrication of PATP-Au_{nano} are assigned to the formation of polaronic and bipolaronic structures of PATP. Thus, we have fabricated a modified catalyst electrode in which Au^0 particles are dispersed without any agglomeration through protection by –SH groups in PATP. Interestingly, we have used cyclic voltammetry to deposit simultaneously the PATP having –SH groups (during anodic potential scans) and Au^0 particles (during cathodic potential scan) on the surface of GC electrode.

Scanning probe microscopic (SPM) measurement reveals the existence of Au^0 nanoparticles in the PATP-Au_{nano}. Fig. 2a and b show the SPM images of CD-ATP-IC and PATP-Au_{nano}, respectively. A relatively high-coverage of ordered monolayer of Au^0 nanoparticles without agglomeration was found on PATP-
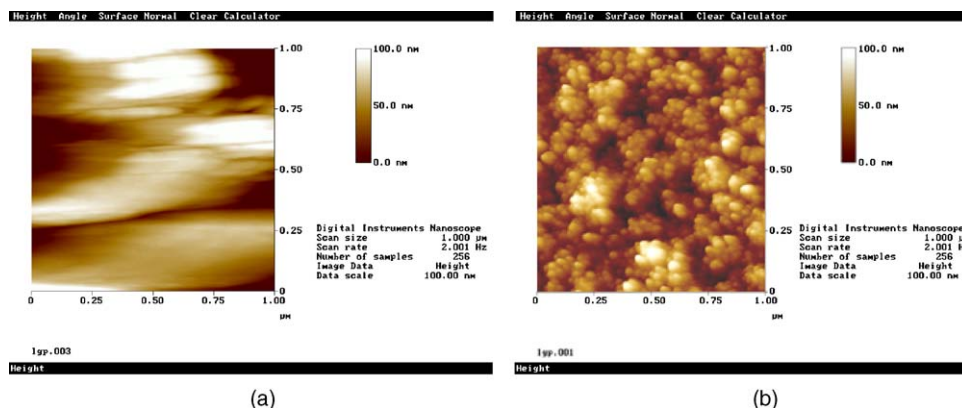

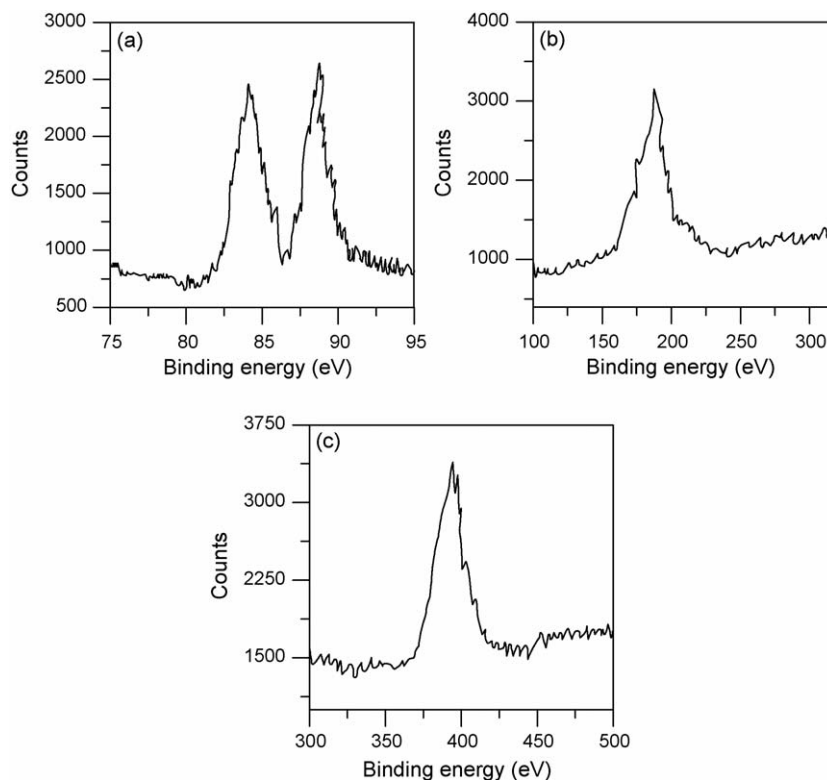Fig. 2. SPM images of GC/CD-ATP-IC (a) and PATP-Au_{nano} catalyst (b).

Fig. 3. XPS spectra of PATP-Au$_{nano}$ catalyst showing (a) the Au(4f 7/2) and Au(4f 5/2) double peaks and (b) S(2p) peak and (c) N(1s) peak.

Au$_{nano}$ with an average size of Au^0 as ∼10–15 nm (Fig. 2b). XPS spectrum of PATP-Au$_{nano}$ (Fig. 3) confirms the presence of Au^0 nanoparticles. The XPS spectrum of PATP-Au$_{nano}$ shows the presence of sulfur (S 2p) and nitrogen (N 1s) peaks at 187.2 and 392.1 eV, respectively. The peaks centered at 83.1 (4f 7/2) and 87.5 eV (4f 5/2) are the signature of Au^0 nanoparticles that exist on PATP-Au$_{nano}$ [38].

Further, catalyst electrodes were fabricated by loading different amounts of Au^0 nanoparticles (15–93 µg cm^{-2}) into the PATP-IC matrix. True surface area, rugosity factor, specific surface area and the size of the Au^0 nanoparticles on the PATP-Au$_{nano}$ catalyst with different loadings of Au^0 particles were determined (Table 1). The specific surface area (cm^2 µg^{-1}) of the catalyst particles was calculated by using the relation,

$$S = \frac{100 A_{rsa}}{W A_{gsa}}$$

where A_{rsa} is the real surface area (as estimated from the charge consumed for the reduction process of the surface oxide monolayer (the peak at ∼920 mV in Fig. 4 and using a reported value of 400 µC cm^{-2} [39–41]), A_{gsa} the geometric surface area ($A_{gsa} = 0.0707$ cm^2) and W (in µg cm^{-2}) is the amount of Au^0 loading. The rugosity factor is the ratio of A_{rsa} to A_{gsa}. Assuming spherical particles of similar radius, the mean particle size of Au^0 particles, d (in nm) was calculated from the following equation:

$$d = \frac{6000}{\rho S}$$

where ρ is the density of Au^0 particle ($\rho = 19.3$ g cm^{-3}) and S is the specific surface area (in cm^2 µg^{-1}).

The PATP-Au$_{nano}$ has shown excellent electrocatalytic activity for the reduction of dioxygen and the details are presented here.

Table 1
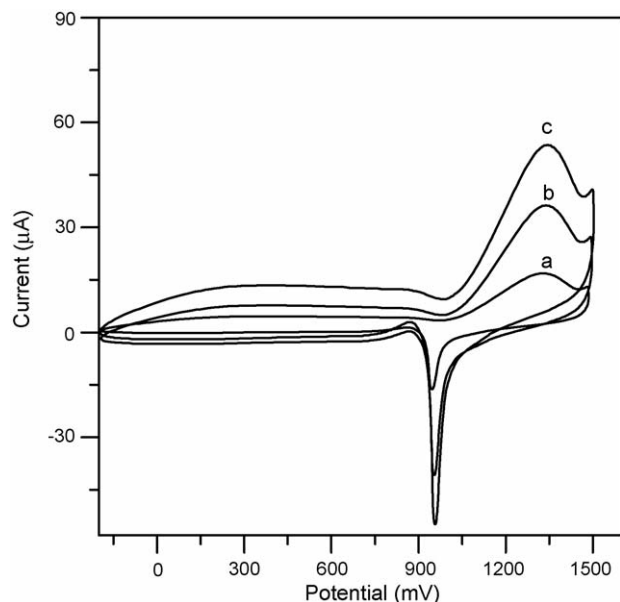Physical characteristics of PATP-Au$_{nano}$ catalyst with different Au^0 loadings

Au loading (µg cm^{-2})	[a]Real surface area of Au loading (cm^{-2})	Rugosity factor	Specific surface area (cm^2 µg^{-1})	Particle size (nm)
15	0.63	8.91	59.40	5
32	0.82	11.59	36.21	9
55	0.98	13.86	25.20	12
78	1.32	18.67	23.93	13
93	1.54	21.78	23.41	13

[a] As estimated from the charge consumed for the reduction peak of the surface oxide monolayer of Au^0 nanoparticles, the peak at ∼920 mV in Fig. 4 using a reported value of 400 µC cm^{-2} [39–41].

Fig. 4. CV response of PATP-Au$_{nano}$ in N$_2$ saturated 0.5 M H$_2$SO$_4$ electrolyte with different Au^0 loadings (a) 32, (b) 55, and (c) 93 μg cm^{-2}.

3.2. Electrocatalytic reduction of dioxygen on the PATP-Au$_{nano}$

Electrocatalytic activity of the PATP-Au$_{nano}$ for oxygen reduction reaction (ORR) was ascertained by recording cyclic voltammograms for the O$_2$ saturated 0.5 M H$_2$SO$_4$ solution. Voltammetric results clearly demonstrated the excellent electroactivity of PATP-Au$_{nano}$ for ORR in comparison to the unmodified GC electrode. Fig. 5A (i and ii) shows the CVs of the PATP-Au$_{nano}$ in O$_2$ saturated and Ar saturated solutions, respectively. A peak at ∼430 mV was observed for the PATP-Au$_{nano}$ for ORR during the cathodic scan of potential (Fig. 5A; line (i)). Comparatively, a reduction wave at ∼300 mV was noticed for ORR on the unmodified GC electrode (Fig. 5B; line (i)). An increased current was also observed at ∼430 mV for the O$_2$ saturated solution. Thus, an enhanced electrocatalytic activity was noticed for PATP-Au$_{nano}$ over the unmodified GC electrode with a positive shift of the O$_2$ reduction potential from 300 to 430 mV and an increase in the current for ORR (Fig. 5A). It is to be noted that a more positive potential for the reduction of O$_2$ and a higher O$_2$ reduction current are the two essential requirements for the catalysts to find utilities in fuel cell applications. The PATP-Au$_{nano}$ also exhibited a lower onset potential for ORR than that reported (0 mV) for (Au$_{nano}$/CoTMPyp)$_6$ multilayer films [42].

The enhanced catalytic activity of the PATP-Au$_{nano}$ for ORR is expected to arise from the small (∼10 nm) crystallite sizes of Au^0 nanoparticles and fine distribution of Au^0 nanoparticles on the surface of PATP film via the formation of Au^0 particles through self-assembly configuration (Scheme 1). Small size (∼10 nm) and uniform distribution of Au^0 nanoparticles are evident from SPM topography (Fig. 2b).

A high surface area is therefore expected due to the uniform distribution of Au^0 nanoparticles. During electrolysis of HAuCl$_4$, Au^0 nanoparticles are preferentially anchored on the
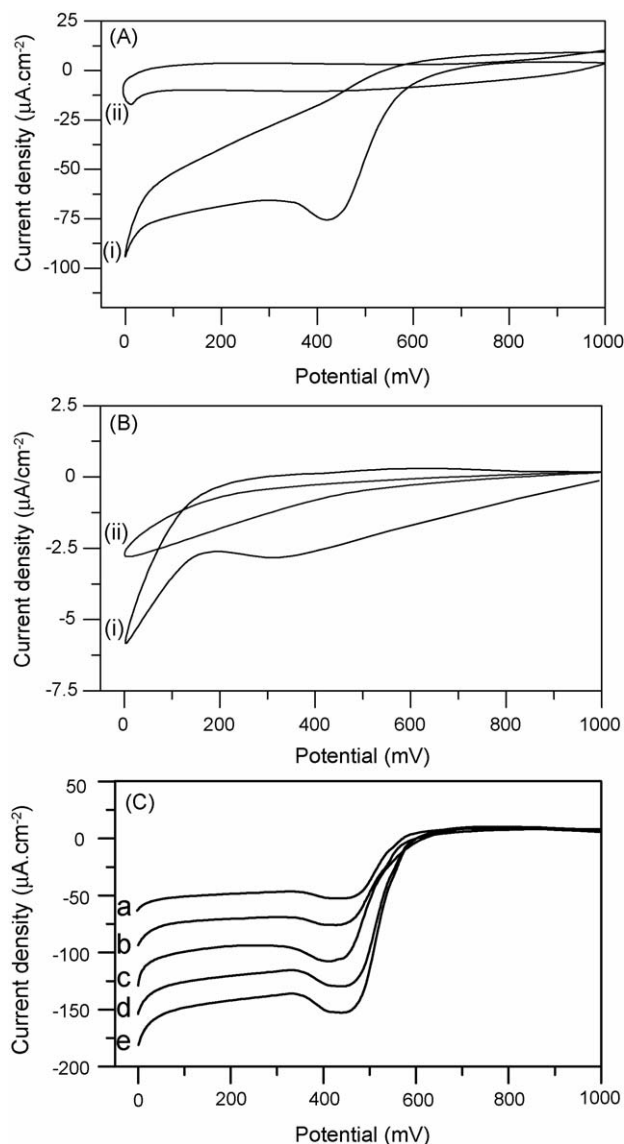

Fig. 5. Cyclic voltammograms of (A) PATP-Au$_{nano}$ and (B) bare GC electrodes in (i) O$_2$ and (ii) Ar saturated 0.5 M H$_2$SO$_4$ electrolyte, respectively; (C) CVs of PATP-Au$_{nano}$ catalyst with different Au^0 loadings in O$_2$ saturated 0.5 M H$_2$SO$_4$ electrolyte; (a) 15, (b) 32, (c) 55, (d) 78 and (e) 93 μg cm^{-2}.

–SH sites (Scheme 1). As a result, the interaction between –SH groups in PATP and Au^0 nanoparticles prevents aggregation of Au^0 nanoparticles. Attachment of Au^0 nanoparticles on to the –SH groups is well known [43–46]. We have also fabricated PATP-Au$_{nano}$ catalysts with different loadings of Au^0 and tested for their electrocatalytic activity towards ORR.

Fig. 5C shows the CVs of the PATP-Au$_{nano}$ with different Au^0 loadings (15–93 μg cm^{-2}) in O$_2$ saturated solution. Current–potential profiles were generated after making corrections for the background current. The correction was executed by subtracting the peak current values recorded in Ar atmosphere from the current values noticed in O$_2$ saturated electrolyte. The voltammograms recorded for ORR on the PATP-Au$_{nano}$ with different Au^0 loadings illustrate a shift in reduction potential for ORR with an increase of Au^0 loading. This infers that over-

potential for ORR decreases and the catalytic activity increases with the increase of Au^0 loading [47].

The kinetics and reaction mechanism of ORR on the PATP-Au_{nano} were investigated through chronoamperometry and hydrodynamic voltammetric experiments and the details of investigation are presented below.

3.3. Chronoamperometry

To get an insight into the dynamics of charge transport on the catalyst electrodes, we have performed a series of chronoamperometry (double potential step) experiments. Fig. 6a shows the chronoamperograms obtained for the PATP-Au_{nano} catalyst with different Au^0 loadings in the presence of O_2. In these cases, first and second working electrode potentials were set
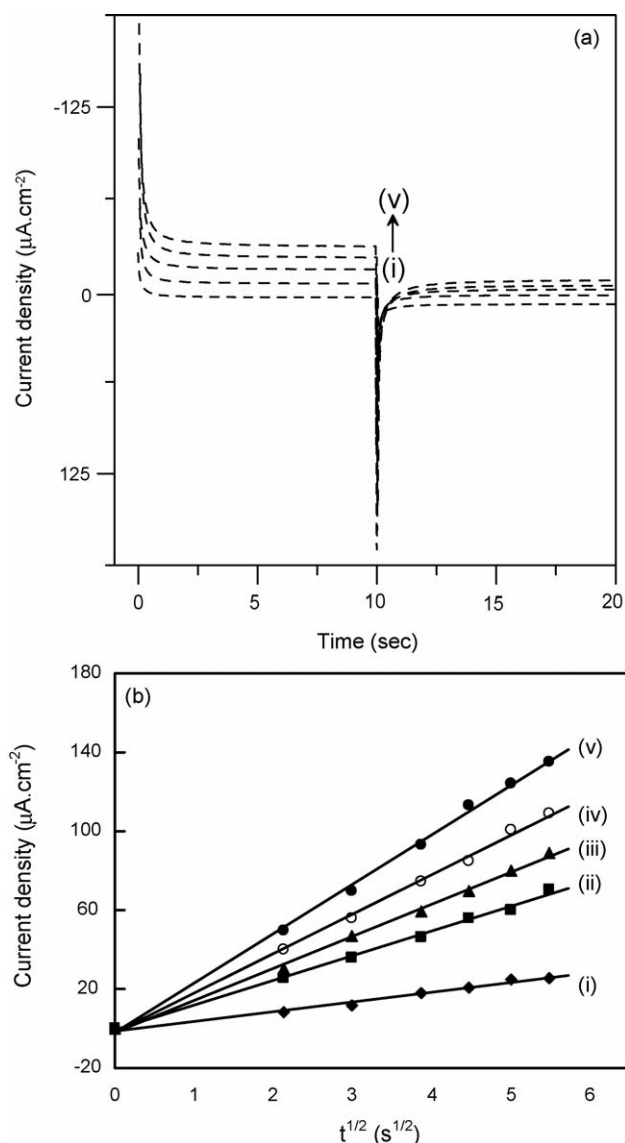
as 800 and 0 mV (versus SCE), respectively. The effective (apparent) diffusion coefficient was estimated from the slopes of dependencies of net electrolysis current (I) versus square root of time ($t^{1/2}$) and using the integrated Cottrell equation [48,49];

$$I = nFAD^{1/2}\frac{c_o}{\pi^{1/2}t^{1/2}}$$

The slope of the plot is $nFAD^{1/2}c_o/\pi^{1/2}$ where n is the number of electrons transferred, F the Faraday constant (96484 C mol^{-1}), A the electrode surface area, c_o the bulk concentration, and D is the diffusion coefficient (cm^2 s^{-1}). Based on Cottrell's equation, the plots of net current, I versus $t^{1/2}$ for different Au^0 loadings were drawn (Fig. 6b). The plot of I versus $t^{1/2}$ is a straight line (Fig. 6b) passing through the origin. The slope of the line gives D as 7.82×10^{-5} cm^2 s^{-1}. The D value obtained for the PATP-Au_{nano} catalyst is comparable with the reported values [50,51]. A value of 1.64×10^{-5} cm^2 s^{-1} for D was reported for ORR on a GC electrode modified by anthraquinone substituted podands [50]. A value of D in the order of 10^{-5} cm^2 s^{-1} was reported for palladium particles dispersed in conducting polymer matrix [51].

The catalytic rate constant (k) for the ORR on the PATP-Au_{nano} was calculated using the method proposed by Galus [52] and using

$$\frac{I_{cat}}{I_l} = \gamma^{1/2}\left[\pi^{1/2}\mathrm{erf}(\gamma^{1/2}) + \frac{\exp(-\gamma)}{\gamma^{1/2}}\right]$$

where I_{cat} is the catalytic current of ORR on the PATP-Au_{nano}, I_l the limiting current in the absence of O_2, and $\gamma = kc_ot$ (c_o is the bulk concentration of O_2) is the argument of the error function. When γ exceeds 2, the error function is almost equal to 1 and therefore the above equation can be reduced to;

$$\frac{I_{cat}}{I_l} = \gamma^{1/2}\pi^{1/2} = \pi^{1/2}(kc_ot)^{1/2}$$

where t is the time elapsed. The slope of I_{cat}/I_l versus $t^{1/2}$ plot gives k as 3.65×10^3 M^{-1} s^{-1}. The rate constant for ORR on the PATP-Au_{nano} catalyst is higher than the one obtained at 1 1 1–1 0 0 nanofaceted platinum surface (2.3×10^2 M^{-1} s^{-1}) [53].

3.4. RDE and RRDE experiments

Kinetics of ORR was followed by using RDE assembly in which the saturation level of O_2 supply to the surface of the electrode was varied by altering the rotation speed of the electrode. The solubility of O_2 (2.293×10^{-5} mol fraction [54] at room temperature in aqueous electrolytes) is quite low for studying the kinetics of ORR in a stationary hanging-meniscus assembly. Hence, we have employed RDE experiments to follow the kinetics of ORR. Fig. 7 shows the hydrodynamic voltammograms recorded at 800 rpm for the ORR on the PATP-Au_{nano} with various Au^0 loadings (15–93 μg cm^{-2}). The current for ORR on the disk electrode commences at ~0.9 V and reaches a limiting value around 0.6 V. The limiting current increases with increasing Au^0 loadings from 15 to 93 μg cm^{-2}. The increase in current for ORR is attributed to arise from the increase active surface area of the catalyst (Table 1).
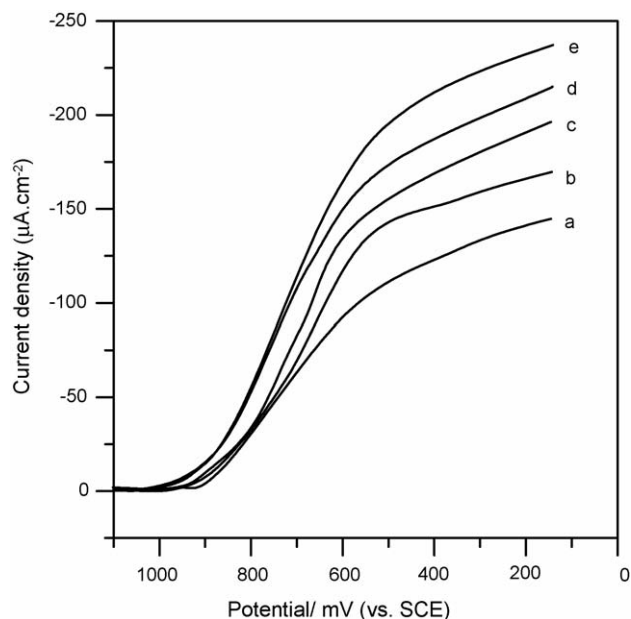
Fig. 6. (a) Chronoamperograms obtained at PATP-Au_{nano} for O_2 saturated 0.5 M H_2SO_4 electrolyte by the double potential-step technique with different amount of Au^0 (i) 15, (ii) 32, (iii) 55, (iv) 78 and (v) 93 μg cm^{-2} and (b) dependence of net current (I) on $t^{1/2}$ derived from the data of double potential chronoamperometry in the presence of O_2.

Fig. 7. $j(E)$ polarization curves for PATP-Au$_{nano}$ in O$_2$ saturated 0.5 M H$_2$SO$_4$ electrolyte for different Au^0 loadings in the presence of O$_2$ (a) 15, (b) 32, (c) 55, (d) 78 and (e) 93 μg cm^{-2} (ω: 800 rpm; temperature = 25 °C; scan rate = 1 mV s^{-1}).

In order to determine the kinetic parameters of ORR on the PATP-Au$_{nano}$ catalyst, polarization curves were recorded for different electrode rotation rates (ω) between 50 and 1000 rpm. Fig. 8 shows the polarization curves of ORR on the PATP-Au$_{nano}$ (Au^0 loading: 78 μg cm^{-2}) recorded for different rotation rates. The current–potential profiles were recorded under
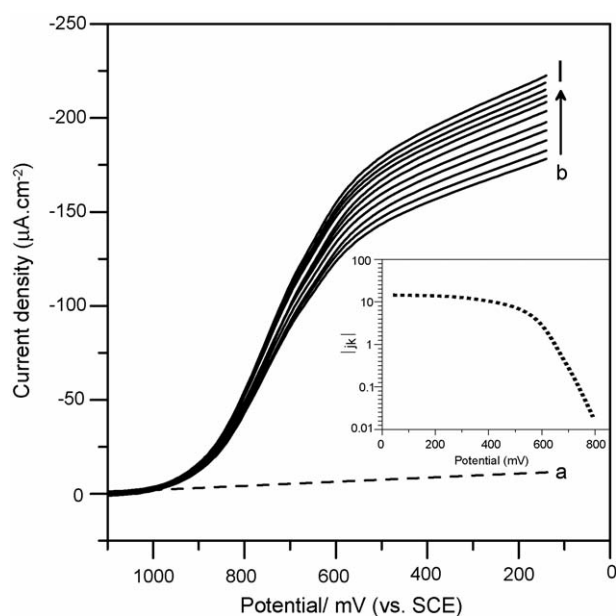
Table 2
Kinetic parameters for the ORR on the PATP-Au$_{nano}$ electrode with different Au^0 loadings

Au loading (μg cm^{-2})	Limiting current density (mA/cm^{-2})	Tafel slope (mV/decade)	Exchange current density (μA/cm^{-2})
15	1.9	120	2.86
32	2.1	112	3.45
55	3.8	116	4.89
78	4.5	128	6.87
93	7.2	135	9.24

quasi-stationary conditions by scanning the potential between 1.1 and 0.0 V versus SCE with a slow scan rate of 1 mV s^{-1}. The limiting current for ORR increases with the rotation rate in the range from 50 to 1000 rpm.

Further insight into the kinetics of the ORR on the PATP-Au$_{nano}$ was deduced from the analysis of Tafel plots (Fig. 8; inset) derived from RDE. The plot of current density, j_k as a function of the electrode potential E was used to determine the limiting current density, j_l. The slope, 'b', was obtained from the Tafel plot (E versus $\ln[j_k/(j_l - j_k)]$). The intercept at the equilibrium potential gives the exchange current density, j_o. The kinetic parameters, j_l, j_o and b obtained for the PATP-Au$_{nano}$ with different Au^0 loadings are presented in Table 2.

The Levich plot (Fig. 9a, current density versus $\omega^{1/2}$) for ORR on the PATP-Au$_{nano}$ is linear and suggests that ORR is a diffusion

Fig. 8. $j(E)$ polarization curves at different rotation rates ω recorded for PATP-Au$_{nano}$ in O$_2$ saturated 0.5 M H$_2$SO$_4$ electrolyte; (a) in the absence of O$_2$ and (b–l) at different rotating rates in presence of O$_2$; (b) 50, (c) 100, (d) 200, (e) 300, (f) 400, (g) 500, (h) 600, (i) 700, (j) 800, (k) 900, and (l) 1000 rpm; (Au^0: 78 μg cm^{-2}; temperature = 25 °C; scan rate = 1 mV s^{-1}) (inset shows the Tafel plot).
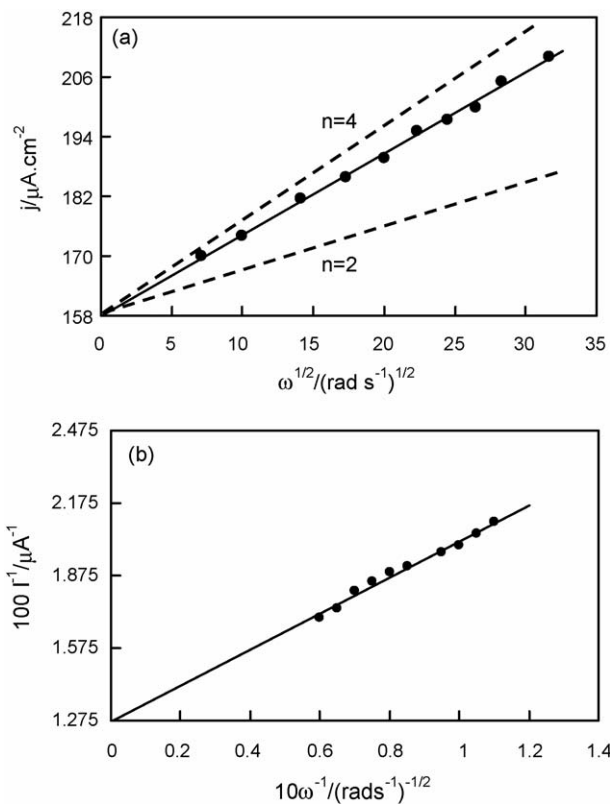

Fig. 9. (a) Levich plot and (b) Koutecky–Levich plot of the kinetic limiting currents of the voltammograms. The solid lines is from the experimental data and the dashed lines are from the calculated data considering the reduction of O$_2$ by four and two electrons, respectively.

controlled process on the PATP-Au$_{nano}$ catalyst. Fig. 9a also reveals that ORR on the PATP-Au$_{nano}$ catalyst is a four electron process and this observation coincides with the theoretical line expected for the four-electron reduction of O_2.

Koutecky–Levich (KL) law is valid for a first-order process with respect to the diffusing species [55], and the current density, j is related to the rotation rate (ω) according to [56,57],

$$\frac{1}{j} = \frac{1}{j_k} + \frac{1}{B\omega^{1/2}}$$

where B is the Levich slope and are given by:

$$j_k = nFAkC_{O_2}$$

$$B = 0.62nF(D_{O_2})^{2/3}\nu^{-1/6}C_{O_2}$$

where D_{O_2} is the diffusion coefficient of dioxygen (7.82×10^{-5} cm^2 s^{-1}), C_{O_2} the solubility of dioxygen (1.03×10^{-3} mol dm^{-3}), ν the kinematic viscosity (1.07×10^{-2} cm^2 s^{-1}) for sulfuric acid, A the area of the electrode, F the Faraday constant, and n is the number of electrons transferred per molecule of O_2.

Information on the reaction paths of ORR was also obtained from the KL plot. In general, the electrode potential that was selected to perform KL analysis, $(j_k)^{-1}$ was obtained from the intercept of the KL plot by extrapolating the ordinate to infinite frequency.

The KL plots for the electrocatalytic ORR on the modified rotating-disk electrodes are presented in Fig. 9b. The linearity and parallel nature of the plot is usually taken as an indication of the first order reaction with respect to dissolved O_2. At high polarizations, slopes over a wide frequency interval is fitted with the calculated behavior of $n = 4$. Through this process, it was identified that the number of electrons involved in ORR is four that is consistent with the Levich analysis (Fig. 9a). For solutions saturated with oxygen, B depends exclusively on the number of electrons (n) consumed per oxygen molecule. In general, the mixed reaction paths are often observed for the reaction involving non-integer number for number of electrons. We have noticed a value close to four for number of electrons that indicates a single step process for ORR. These results therefore confirm that overall ORR is a four electron process and is given by,

$$O_2 + 4H^+ + 4e^- \rightarrow 2H_2O$$
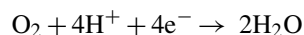
It is known [58] that the direct 4e$^-$ path for ORR is favored on surfaces that enable the dissociation of adsorbed O_2, i.e. in the cases when adsorption forces are equally distributed to both oxygen atoms. If one atom of a molecule is more strongly bonded than the other, the dissociation is aggravated and the indirect, 2e$^-$ reduction path is favored. A 2e$^-$ reduction path for ORR was reported for a Au-CoTMPyP modified GC electrode [42]. Earlier reports indicated that differences in the surface structure of the nanoparticles may influence the electrocatalytic behavior of the nanoparticles. Surface structure of the nanoparticles is decided by the modifier used during the preparation of the nanoparticles and the electrochemical ORR occurs accordingly on the catalyst surface [60]. Hernandez et al. [60] used

the adsorbates such as iodide and sulfide (surface modifiers) during the synthesis of Au nanoparticles. Iodide induces the formation of (1 1 1) or (1 0 0) facets Au, whereas sulfide induces (1 1 0) facet Au. A four electron path for ORR was predominant on the Au(1 0 0) surface, whilst, the number of electrons for the ORR was found to be two on the Au(1 1 0) surface [60]. In the case of the Au-CoTMPyP modified GC electrode [42], a [tetrakis(N-methylpyridyl)porphyrinato] cobalt (CoTMPyP) anion was used during the formation of Au nanoparticles and a 2e$^-$ for ORR was witnessed. In the present study, it is presumed that Au nanoparticles are distributed in the network of PATP, a conducting polymer. Hence, the observed 4e$^-$ path for ORR is presumably due to the presence of PATP as a modifier for Au nanoparticles.

In the present study, adsorption forces of both oxygen atoms may be considered equally distributed onto the catalytic surface of Au^0. The electrocatalyst predominantly favors the formation of water than hydrogen peroxide through the 4e$^-$ path. A similar 4e$^-$ reduction path for ORR was reported for the Au^0 nanoparticles prepared in the presence of cysteine [59]. A 4e$^-$ reduction path was reported for the ORR on Au^0 nanoparticles synthesized in a water-in-oil microemulsion with potassium iodide [60].

Rotating GC electrode, modified with PATP-Au$_{nano}$ as disk and platinum ring electrode were used to carry out RRDE experiments. Quantity of H_2O_2 that was generated during the reduction process of O_2 on the rotating disk electrode was determined. This provides further supports for the effectiveness of the catalyst for the proposed four-electron reduction of dioxygen. Fig. 10 shows the voltammetric curves for dioxygen reduction, recorded at the RRDE with the PATP-Au$_{nano}$ modified GC disk electrode. The disk potential was scanned from 1.1 to 0 V, while the ring potential was kept at 1.0 V to oxidize the H_2O_2 generated by O_2 reduction on the disk electrode. A large disk current
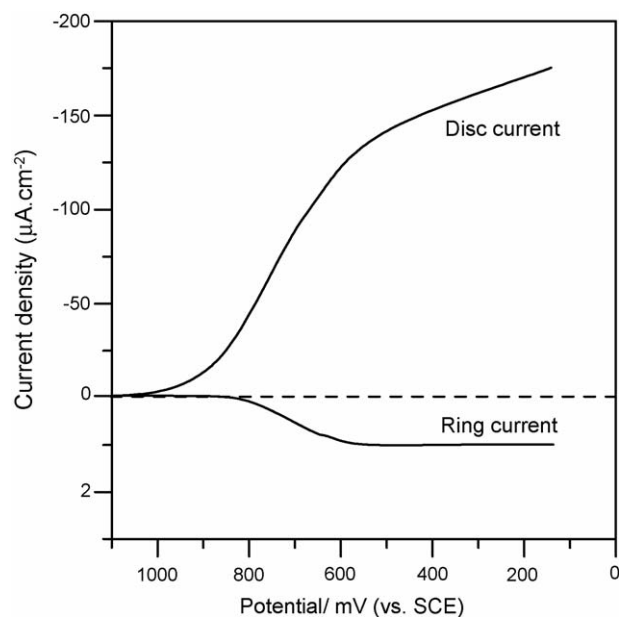

Fig. 10. Current–potential curves for the O_2 reduction in O_2 saturated 0.5 M H_2SO_4 electrolyte at PATP-Au$_{nano}$ modified GC rotating disk electrode (Au^0: 78 μg cm^{-2}) and platinum ring electrode at $\omega = 100$ rpm; $E_R = 1.0$ V vs. SCE.

was observed for the PATP-Au$_{nano}$ modified GC disk electrode (Fig. 10). The ratio of the ring to disk current, i_R/i_D, is found to be 0.005 for the modified electrode. From the ratio of the ring–disk currents, the number of electrons involved in ORR is found to be 4 [61], which is consistent with the values obtained from the Levich and KL plot.

Taking into account that the rates of formation of H_2O_2 and H_2O are i_R/N and $i_D - i_R/N$, respectively, the formation efficiency of H_2O was estimated as follows [62];

$$P_{(H_2O)} = \frac{N(i_D/i_R) - 1}{N(i_D/i_R) + 1}$$

From the value of i_R/i_D, the efficiency of H_2O formation for the PATP-Au$_{nano}$ catalyst was found to be 92%. This result indicates that the reduction of dioxygen on the PATP-Au$_{nano}$ catalyst mainly supports the $4e^-$ pathway to produce a high yield of H_2O.

3.5. Stability of PATP-Au$_{nano}$ catalysts

We checked the stability of the PATP-Au$_{nano}$ electrode by measuring the current response of the catalyst for ORR for few days by storing the electrode in the electrolyte solution at 25 °C. There was no apparent decrease in the current response for the first 2 days. In the next 2 days, a decrease of 3% of its initial value in the current response was noticed. After a week, a decrease of 4% in current response was witnessed. The results demonstrate the good stability of PATP-Au$_{nano}$.

4. Conclusions

New catalysts comprising of gold nanoparticles uniformly distributed into conducting poly(aminothiophenol), PATP matrix are developed by cyclic electrochemical process and a modified electrode was fabricated. The PATP-Au$_{nano}$ catalyst electrode has an enhanced electrocatalytic activity for oxygen reduction reaction and proves to be promising for its utility in fuel cells, O_2 sensor, etc. Importantly, the PATP-Au$_{nano}$ catalyst can be formed on any substrate (hydrophobic (glassy carbon), hydrophilic (indium tin oxide) or electroactive membranes) using the methodology developed in the present investigation. Further, PATP-Au$_{nano}$ catalysts are expected to find useful for other electrochemical or chemical reactions.

References

[1] L. Sheeney-Haj-Ichia, G. Sharabi, I. Willner, Adv. Funct. Mater. 12 (2002) 27.

[2] M. Hepel, J. Electrochem. Soc. 145 (1998) 124.

[3] P.J. Kulesza, M. Chojak, K. Karnicka, K. Miecznikowski, B. Palys, A. Lewera, A. Wieckowski, Chem. Mater. 16 (2004) 4128.

[4] S. Tian, J. Liu, T. Zhu, W. Knoll, Chem. Mater. 16 (2004) 4103.

[5] V.P. Yissar, T. Bourenko, J. Wasserman, I. Willner, Adv. Mater. 14 (2002) 670.

[6] L. Zhang, M. Wan, J. Phys. Chem. B 107 (2003) 6748.

[7] L.H. Mascaro, D. Goncalves, L.O.S. Bulhoes, Thin Solid Film 461 (2004) 243.

[8] P. Santhosh, A. Gopalan, Kwang-Pill Lee, J. Catal. 238 (2006) 177.

[9] M. Valden, X. Lai, D.W. Goodman, Science 281 (1998) 1647.

[10] L.O. Brown, J.E. Hutchison, J. Phys. Chem. B 105 (2001) 8911.

[11] R.L. Whetten, J.T. Khoury, M.M. Alvarez, S. Murthy, I. Vezmar, Z.L. Wang, P.W. Stephens, C.L. Cleveland, W.D. Luedtke, U. Landman, Adv. Mater. 8 (1996) 428.

[12] M. Brust, M. Walker, D. Bethell, D.J. Schiffrin, R. Whyman, J. Chem. Soc., Chem. Commun. (1994) 801.

[13] M.S. El-Deab, T. Ohsaka, Electrochem. Commun. 4 (2002) 288.

[14] M.S. El-Deab, T. Ohsaka, Electrochim. Acta 47 (2002) 4255.

[15] S. Schimpf, M. Lucas, C. Mohr, U. Rodemerck, A. Bruckner, J. Radnik, H. Hofmeister, P. Claus, Catal. Today 72 (2002) 63.

[16] M. Haruta, Catal. Today 36 (1997) 153.

[17] A. Dekanski, J. Stevanovic, R. Stevanovic, B.Z. Nikolic, V.M. Jovanovic, Carbon 39 (2001) 1195.

[18] D. Martel, A. Kuhn, Electrochim. Acta 45 (2000) 1829.

[19] A. Sarapuu, K. Tammeveski, T.T. Tenno, V. Sammelselg, K. Kontturi, D.J. Schiffrin, Electrochem. Commun. 3 (2001) 446.

[20] J. Schulz, A. Roucoux, H. Patin, Chem. Rev. 102 (2002) 3757.

[21] O.V. Cherstiouk, P.A. Simonov, E.R. Savinova, Electrochim. Acta 48 (2003) 3851.

[22] S. Liu, T. Zhu, R. Hu, Z. Liu, Phys. Chem. Chem. Phys. (2002) 6059.

[23] J. Matsui, K. Akamatsu, S. Nishiguchi, D. Miyoshi, H. Nawafune, K. Tamaki, N. Sugimoto, Anal. Chem. 76 (2004) 1310.

[24] E.S. Forzani, H. Zhang, L.A. Nagahara, I. Amlani, R. Tsui, N. Tao, Nano Lett. 4 (2004) 1785.

[25] T. Osaka, S. Ogano, K. Naoi, N. Oyama, J. Electrochem. Soc. 136 (1989) 306.

[26] B. Srinivas, United States Patent 20,040,166,401 (2004).

[27] E.W. Paul, A.J. Ricco, M.S. Wrighton, J. Phys. Chem. 89 (1985) 1441.

[28] M.A. Breimer, G. Yevgeny, S. Sy, O.A. Sadik, Nano Lett. 1 (2001) 305.

[29] P. Santhosh, A. Gopalan, T. Vasudevan, Kwang-Pill Lee, Appl. Sur. Sci., in press.

[30] M. Sastry, Curr. Sci. 78 (2000) 1089.

[31] F.P. Zamborini, J.F. Hicks, R.W. Murray, J. Am. Chem. Soc. 122 (2000) 4514.

[32] A. Mamedov, J. Ostrander, F. Aliev, N.A. Kotov, Langmuir 16 (2000) 3941.

[33] J. Schmitt, G. Decher, W.J. Dressich, S.L. Brandow, R.E. Geer, R. Shashidhar, J.M. Calvert, Adv. Mater. 9 (1997) 61.

[34] K.V. Sarathy, P.J. Thomas, G.U. Kulkami, C.N.R. Rao, J. Phys. Chem. B 103 (1999) 399.

[35] A. Harada, M. Kamachi, Nature 356 (1992) 325.

[36] M.O. Finot, G.D. Braybrook, M.T. McDermott, J. Electroanal. Chem. 466 (1999) 234.

[37] M. Okamura, T. Kondo, K. Uosaki, J. Phys. Chem. B 109 (2005) 9897.

[38] G. Lu, D. Ji, G. Qian, Y. Qi, X. Wang, J. Suo, Appl. Catal. A 280 (2005) 175.

[39] A.A. Michri, A.G. Pshchenichikov, Kh.R. Burshtein, Sov. Electrochem. 8 (1972) 351.

[40] S. Trasatti, O.A. Petrii, Pure Appl. Chem. 63 (1991) 711.

[41] H.A. Kozlowska, B.E. Conway, A. Hamelin, L. Stoicoviciu, J. Electroanal. Chem. (1987) 429.

[42] M. Huang, Y. Shen, W. Cheng, Y. Shao, X. Sun, B. Liu, S. Dong, Anal. Chim. Acta 535 (2005) 15.

[43] A. Badia, L. Demers, L. Dickinson, F.G. Morin, R.B. Lennox, L. Reven, J. Am. Chem. Soc. 119 (1997) 11104.

[44] N.R. Jana, X. Peng, J. Am. Chem. Soc. 125 (2003) 14280.

[45] M.J. Hostetler, J.E. Wingate, C.J. Zhong, J.E. Harris, R.W. Vachet, M.R. Clark, J.D. Londono, S.J. Green, J.J. Stokes, G.D. Wignall, G.L. Glish, M.D. Porter, N.D. Evans, R.W. Murray, Langmuir 14 (1998) 17.

[46] W.A. Hayes, C. Shannon, Langmuir 12 (1996) 3688.

[47] S. Ye, A.K. Vijh, Electrochem. Commun. 5 (2003) 272.

[48] A.J. Bard, L.R. Faulkner, Electrochemical Methods: Fundamentals and Applications, second ed., Wiley, 2001.

[49] P.J. Kulesza, M.A. Malik, In: A. Wieckowski (Ed.), Interfacial Electro-chemistry, Marcel Dekker.

[50] A. Salimi, H. Eshghi, H. Sharghi, S.M. Golabi, M. Shamsipur, Electro-analysis 11 (1991) 114.

[51] A. Yassar, J. Roncali, F. Garnier, J. Electroanal. Chem. 255 (1998) 53.

[52] Z. Galus, Fundamentals of Electrochemical Analysis, Ellis Horwood Press, New York, 1976, p. 313 (Chapter 10).

[53] V. Komanicky, A. Menzel, H. You, J. Phys. Chem. B 109 (2005) 23550.

[54] D.R. Lide (Ed.), CRC Handbook of Chemistry and Physics, 85th ed., CRC Press, Boca Raton, FL, 2004.

[55] A.J. Bard, L.R. Faulkner, Electrochemical Methods: Fundamentals and Applications, Wiley, New York, 1980.

[56] K. Tammeveski, T. Tenno, A. Rosental, P. Talonen, L.S. Johansson, L. Niinisto, J. Electrochem. Soc. 146 (1999) 669.

[57] N.A. Anastasijevic, Z.M. Dimitrijevic, R.R. Adzic, Electrochim. Acta 31 (1986) 1125.

[58] C.H. Hamann, A. Hamnett, W. Vielstich, Electrochemistry, Wiley WCH, 1998, p. 281.

[59] M.S. El-Deab, T. Sotomura, T. Ohsaka, Electrochem. Commun. 7 (2005) 29.

[60] J. Hernandez, J. Solla-Gullon, E. Herrero, J. Electroanal. Chem. 574 (2004) 185.

[61] S. Liu, J. Xu, H. Sun, D. Li, Inorg. Chim. Acta 306 (2000) 87.

[62] R.C.M. Jakobs, L.J.J. Janssen, E. Barendrecht, Electrochim. Acta 30 (1985) 1085.